



Experimental and Theoretical Study of Corrosion Behaviour of Maraging Steel in 1 M HCl in Presence of 5-Methyl-4-[(E)-(thiophen-2-ylmethylidene)amino]-4H-1,2,4-triazole-3-thiol

R.N. MARY¹, R. NAZARETH¹, P. KRISHNA MURTHY² and P.A. SUCHETAN^{3,*}

¹Department of Chemistry, St. Aloysius College, Mangaluru-575003, India

²Department of Chemistry, Bapatla Engineering College (Autonomous), Bapatla-522102, India

³Department of Studies and Research in Chemistry, University College of Science, Tumkur University, Tumkur-572103, India

*Corresponding author: E-mail: pasuchetan@gmail.com

Received: 26 September 2019;

Accepted: 27 November 2019;

Published online: 25 February 2020;

AJC-19802

The inhibitory action of a synthesized Schiff base (5-methyl-4-[(E)-(thiophen-2-ylmethylidene)amino]-4H-1,2,4-triazole-3-thiol) [MTATT] on the corrosion behaviour of maraging steel in 1 M HCl was investigated by electrochemical techniques like Tafel polarization studies and electrochemical impedance spectroscopy. According to experimental data, inhibition efficiency increased with increase in temperature and concentration of the inhibitor where MTATT acts as a mixed type inhibitor. The mode of inhibitor adsorption on maraging steel follows Langmuir adsorption isotherm. The calculated thermodynamic and activation parameters suggested chemisorption mode of inhibitor adsorption. Scanning electron microscope technology with energy dispersive X-ray spectroscopy (SEM-EDX) studies confirmed the adsorption of inhibitor molecule on the surface of maraging steel. Several global reactivity parameters were calculated using DFT method at B3LYP/6-311++(d,p) basis set. Theoretical calculations are in good concurrence with the experimental results.

Keywords: Maraging steel, Schiff base, Potentiodynamic polarization, EIS, Inhibition efficiency.

INTRODUCTION

Corrosion, even though a natural process is a destructive phenomenon which results in material degradation leading to enormous losses in industry and society. Corrosion inhibition study of iron and iron alloys is of immense importance due to its wide applications in industry, domestic life and as construction material in many industries due to its excellent mechanical properties and low cost [1,2]. Since metals and alloys frequently come in contact with water, acids, bases, salts, oils and certain chemicals they are likely to undergo corrosion [3-5]. One of the practical methods of protecting metals against corrosion involves the use of corrosion inhibitors. According to surface chemistry, the surface reactions are affected by the presence of foreign molecules. Corrosion being a surface phenomenon, can be controlled by foreign compounds called inhibitors. Inhibitors are substances which when used at low concentrations retard or delay corrosion by getting adsorbed on the reacting metal surface [6]. It may block the active sites of

corrosion and limit the rate of anodic and cathodic process or may increase the electrode potential.

Organic compounds containing atoms such as N, O, S, etc. having lone pair of electrons and also compounds containing electronegative functional groups and electrons in triple and conjugated double bonds have been found to be effective corrosion inhibitors [7-10].

Maraging steel is a low carbon steel containing 18 wt % Ni, substantial amounts of Co and Mo along with small amounts of Ti. Maraging steel is distinguished with outstanding mechanical properties, workability and heat treatment characteristics. The mechanical property is due to the heat treatment performed to bring about precipitation of intermetallics in the Fe-Ni martensitic matrix [11]. Maraging steels are identified with high ductility, formability, corrosion resistance, high strength and ease of fabrication, weldability and maintenance of invariable size even after heat treatment [12]. The application areas of maraging steel include missile and rocket motor cases, landing and takeoff gear, aerospace, extrusion tooling, die

casting, high performance shafting, *etc.* Acid solutions are used in cleaning, pickling, descaling, acidizing, *etc.* and maraging steels does come in contact with acids during such processes and hence is subjected to corrosion.

Literature review shows 18 % Ni maraging steel, due to atmospheric exposure gets completely covered with rust as a result of uniform corrosion [13]. The effect of carbonate ions in slightly alkaline medium on the corrosion of maraging steel has been reported [14]. The inhibitory effect of aminophenyl-tetrazole and 5-(3-aminophenyl)-tetrazole on corrosion behaviour of maraging steel in acid medium has been studied and reported with good inhibition efficiency [15,16]. The effect of 1-(2*E*)-1-(4-aminophenyl)-3-(2-thienyl)prop-2-en-1-one on the corrosion resistance of maraging steel has been studied and shown that the efficiency increases with increase in concentration of the inhibitor [17]. In previous work, we have studied the corrosion inhibition of maraging steel in hydrochloric acid medium using a Schiff base 4-[[4-(dimethylamino)benzylidene]amino]-5-methyl-4*H*-1,2,4-triazole-3-thiol [DBAMTT] [18,19]. The Schiff base showed an increase in inhibition property with increasing temperature and reported an inhibition efficiency of 81 % at 45 °C [18]. The same Schiff base has also been studied for its inhibition property on 316 stainless steel in 2 M HCl medium and has shown good inhibition efficiency [19]. Since Schiff bases can be synthesized by condensing triazoles with aldehydes, for the present study similar Schiff base was synthesized by changing the aldehyde moiety and inhibitory action of the synthesized inhibitor was studied in 1 M HCl.

EXPERIMENTAL

Synthesis of [5-methyl-4-(*E*)-(thiophen-2-ylmethylidene)-amino]-4*H*-1,2,4-triazole-3-thiol: The inhibitor was synthesized as per the reported procedure by preparing triazole from glacial acetic acid and thiocarbonylhydrazide [20,21]. The synthesized triazole was refluxed with thiophene-2-aldehyde in absolute alcohol to obtain the required Schiff base. The product formed was filtered dried and recrystallized from ethanol. Melting point of the synthesized inhibitor was in the range 160-162 °C.

Medium: AnalaR grade 35 % HCl was diluted using double distilled water in order to prepare standard solutions of 1 M HCl. Corrosive medium of 1 M HCl in the absence and with inhibitor concentrations of 10, 100, 200 and 300 ppm were employed for the present corrosion study. Temperature range used for the study was 30-45 °C using calibrated thermostat.

The material used for the study was 18 % Ni M250 grade maraging steel with percentage composition as given in Table-1.

TABLE-1
PERCENTAGE COMPOSITION OF 18 %
Ni M250 GRADE MARAGING STEEL

Element	Composition	Element	Composition
C	0.015 %	Ti	0.3-0.6 %
Ni	17-19 %	Al	0.05-0.15 %
Mo	4.6-5.2 %	Mn	0.1 %
Co	7-8.5 %	P	0.01 %
Si	0.1 %	S	0.01 %
O	30 ppm	N	30 ppm
H	2.0 ppm	Fe	Balance

The working electrode used for the present study was cut from a plate into a rod and molded with epoxy resin with an open surface area of 0.8910 cm² to be immersed in acid medium. According to the standard metallographic practice, the test coupon was polished by subjecting it to belt grinding followed by abrading over emery papers of different grades and subsequently on a polishing wheel using legated alumina abrasive to obtain mirror finish. The abraded specimen was washed with distilled water, degreased with acetone and dried prior to immersion in acid medium.

Electrochemical measurements: Electrochemical measurements namely Tafel polarization and electrochemical impedance spectroscopy were performed using an electrochemical work station, Gill AC having ACM instrument Version 5 software. The electrochemical cell constituted a three-electrode compartment glass cell having saturated calomel electrode (SCE) as reference electrode, platinum as counter electrode and specimen of maraging steel as the working electrode. In order to attain a steady state open circuit potential (OCP), the working electrode after fine polish and drying was immersed in corrosive medium of 1 M HCl without and with the inhibitor at different temperatures (30-45 °C).

Electrochemical impedance spectroscopy (EIS) measurements were performed over a frequency range of 10 kHz to 0.01 Hz by applying a AC signal Amplitude of 10 mV to the electrical system. Potentiodynamic polarization curves were recorded soon after impedance measurements. Polarization studies were performed by polarizing the specimen from -250 mV cathodically to +250 mV anodically with respect to OCP at a scan rate of 1 mV/s.

Scanning electron microscopy-energy dispersive X-ray spectroscopy (SEM-EDX): SEM-EDX analyses of corroded and inhibited maraging steel specimen immersed in 1 M HCl solution were recorded in order to analyze the surface morphology of the specimen. Analysis was carried out using SEM-EDX studies (Carl Zeiss, USA) and (Oxford Instruments).

Quantum chemical calculations: To get further insight into the effect of molecular structure, electronic and reactivity properties of the title inhibitor, the geometry was optimized in ground state in gas phase. All calculations were performed within the density functional theory (DFT) with exchange correlation hybrid functional: B3LYP (three-parameter exchange functional of Becke B3 [22] combined with the Lee-Yang-Parr correlation functional LYP [23] using the extended basis sets with polarization and diffuse functions 6-311++G(d,p) by using Gaussian 09 software package [24]. For acuminous visualization, we employ the package GaussView [25].

RESULTS AND DISCUSSION

Tafel polarization measurements: Tafel plots for maraging steel specimen immersed in 1 M HCl solution in the absence and presence of inhibitor at different temperatures were recorded and results were tabulated. Tafel Polarization curves for corrosion of maraging steel in 1 M HCl at 40 °C with different inhibitor concentrations is shown in Fig. 1.

Tafel parameters like corrosion potential (E_{corr}), corrosion current density (i_{corr}), cathodic slope (β_c), corrosion rate (v_{corr}) and inhibition efficiency (η) were given in Table-2.

TABLE-2
RESULTS OF TAFEL POLARIZATION STUDIES ON MARAGING STEEL IN
1 M HCl CONTAINING DIFFERENT CONCENTRATIONS OF THE INHIBITOR

Temperature (°C)	Concentration of inhibitor (ppm)	E_{corr} (mV/SCE)	$-\beta_c$ (mV dec ⁻¹)	i_{corr} (mA cm ⁻²)	v_{corr} (mm y ⁻¹)	η (%)
30	Blank	-261.63	122.46	1.9963	25.0181	–
	10	-270.30	133.57	0.8194	10.2701	58.94
	100	-262.44	123.77	0.7473	9.3662	62.56
	200	-260.55	85.941	0.6754	8.4649	66.16
	300	-269.19	132.54	0.5902	7.3970	70.43
35	Blank	-257.41	149.24	3.4194	42.8527	–
	10	-279.40	152.12	1.0581	13.2603	69.05
	100	-269.12	108.92	0.9090	11.3926	73.41
	200	-266.02	141.16	0.7465	9.3559	78.16
	300	-279.39	140.69	0.6938	8.6951	79.70
40	Blank	-257.29	177.38	5.8364	73.1432	–
	10	-275.95	150.91	1.3999	17.5438	76.01
	100	-263.95	137.76	1.2067	15.1226	79.32
	200	-281.96	160.36	0.9479	11.8797	83.75
	300	-285.91	148.24	0.7405	9.2803	87.31
45	Blank	-255.26	177.63	9.4538	118.477	–
	10	-277.94	165.12	2.0515	25.7099	78.29
	100	-269.58	102.79	1.7614	22.0743	81.36
	200	-271.77	126.08	1.5046	18.8560	84.08
	300	-279.09	148.08	0.8779	11.0027	90.71

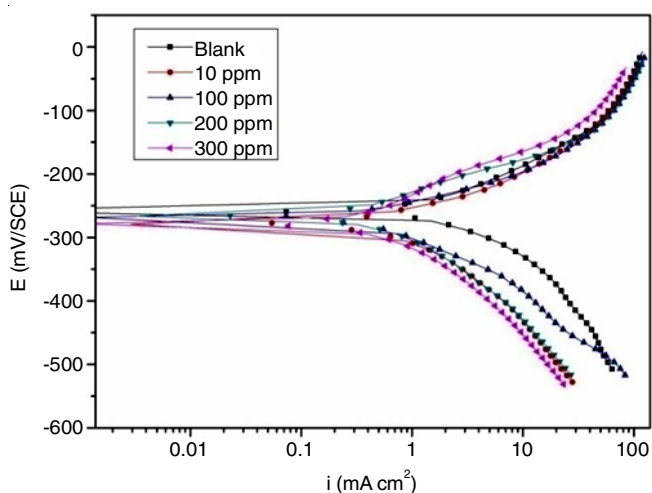


Fig. 1. Tafel polarization curves for the corrosion of maraging Steel in 1 M HCl containing different concentrations of inhibitor at 40 °C

The corrosion rate was calculated using eqn. 1 [26]:

$$v_{\text{corr}} (\text{mm y}^{-1}) = \frac{3270 \times M \times i_{\text{corr}}}{\rho \times Z} \quad (1)$$

where, 3270 is a constant that defines unit of corrosion rate, i_{corr} is corrosion current density, ρ is the density of corroding material, M is the atomic mass of the metal and Z is number of electrons transferred per atom.

The inhibition efficiency was calculated from eqn. 2 [27]:

$$\eta (\%) = \frac{i_{\text{corr}} - i_{\text{corr}}(\text{inh})}{i_{\text{corr}}} \times 100 \quad (2)$$

where, i_{corr} and $i_{\text{corr}}(\text{inh})$ are corrosion current densities obtained in uninhibited and inhibited solutions.

Table-2 indicates increased rate of corrosion with rise in temperature in the absence of the inhibitor. The addition of the inhibitor resulted in decrease in corrosion rate. With increasing

temperature and inhibitor concentration an increase in inhibition efficiency was observed. The addition of the inhibitor did not show a definite shift in E_{corr} values with respect to blank solution. A displacement in corrosion potential (E_{corr}) of more than ± 85 mV with respect to the corrosion potential of the blank is required for an inhibitor to be categorized distinctly as cathodic or anodic type. The present study shows a maximum displacement of about ± 28 mV indicating that MTATT behaves as a mixed type inhibitor affecting both metal dissolution and hydrogen evolution reactions [28]. With increase in inhibitor concentration it was noticed that cathodic polarization curves did not show much variation indicative of the fact that hydrogen evolution is activation controlled and presence of inhibitor does not alter the inhibition mechanism [29,30].

Electrochemical impedance spectroscopy: EIS is a useful technique in understanding the mechanism of corrosion. The effect of inhibitor concentration on impedance behaviour of maraging steel was studied and results were compared with Tafel polarization studies. Fig. 2 represents Nyquist plots for maraging steel in 1 M HCl at 40 °C using different concentrations of the inhibitor.

Nyquist plots are characterized by a large semi-circular capacitive loop at high frequency range (HF). The diameter of the Nyquist plots showed an increase as the inhibitor concentration increased suggesting a decrease in corrosion rate [31]. The high frequency capacitive loop is often attributed to the charge-transfer between the alloy and the electrolyte. Similar plots in the absence and presence of the inhibitor suggests that the inhibitor does not alter the corrosion mechanism. The deviation from the perfect semicircular nature of Nyquist plots is attributed to in homogeneity and impurities of the solid electrode surface [32].

Depending on the shape of Nyquist plots the impedance data was analyzed using suitable equivalent circuit. The circuit fitting was done using ZSimpWin 3.21 software and results

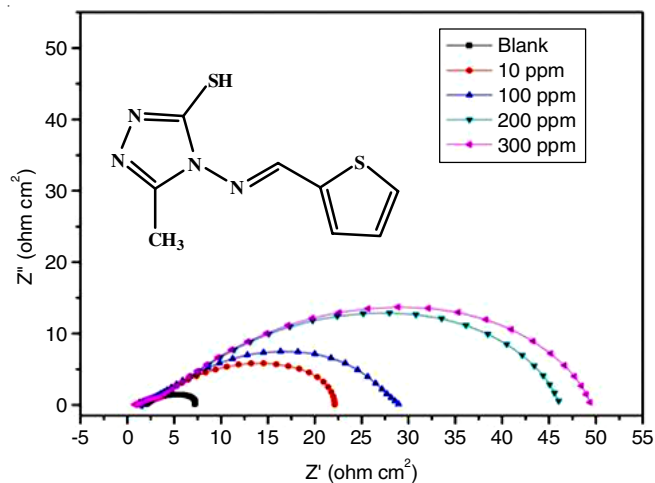


Fig. 2. EIS curves for the corrosion of maraging steel in 1 M HCl containing different concentrations of inhibitor at 40 °C

obtained are listed in Table-3. A simplified Randles circuit (Fig. 3) was used to fit the results as it provided the best fit.

TABLE-3 RESULTS OF EIS STUDIES ON MARAGING STEEL IN 1 M HCl CONTAINING DIFFERENT CONCENTRATIONS OF THE INHIBITOR				
Temp. (°C)	Concentration of inhibitor (ppm)	R_{ct} (ohm cm^2)	$C_{dl} \times 10^3$ ($F cm^2$)	η (%)
30	Blank	11.38	27.57	–
	10	37.80	14.10	69.89
	100	43.30	18.30	73.71
	200	49.70	20.46	77.10
	300	53.30	12.99	78.64
35	Blank	7.44	42.11	–
	10	33.60	9.38	77.85
	100	37.70	10.61	80.26
	200	47.40	13.06	84.30
	300	50.10	11.49	85.14
40	Blank	5.79	48.19	–
	10	22.7	11.35	74.49
	100	29.4	16.15	80.30
	200	44.3	9.75	86.93
	300	48.9	9.38	88.15
45	Blank	3.31	72.91	–
	10	18.0	9.36	81.61
	100	20.7	11.45	84.00
	200	25.5	13.62	87.01
	300	41.4	9.63	92.00

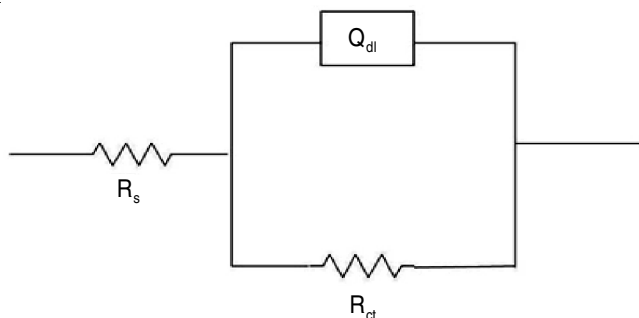


Fig. 3. Equivalent circuit used to fit experimental EIS data

The circuit consists of a solution resistance R_s , charge-transfer resistance R_{ct} and a constant phase element correspon-

ding to double layer, Q_{dl} . In the equivalent-circuit, a constant phase element was used in the place of ideal capacitor to give a more accurate fit.

The charge transfer resistance is inversely proportional to corrosion current density as given by Stern-Geary equation (eqn. 3) [33]:

$$i_{corr} = \frac{b_a b_c}{2.303(b_a + b_c)R_{ct}} \quad (3)$$

Inhibitor efficiency (η , %), was calculated from the following relationship (eqn. 4) [34]:

$$\eta (\%) = \frac{R_{ct(inh)} - R_{ct}}{R_{ct(inh)}} \times 100 \quad (4)$$

where, $R_{ct(inh)}$ and R_{ct} are the charge transfer resistances obtained in inhibited and uninhibited solutions, respectively.

The CPE element is used to explain depression of the capacitance semicircle. The CPE impedance (Z_{CPE}) is given by the expression:

$$Z_{CPE} = \frac{1}{Q} \times \frac{1}{(j\omega)^n} \quad (5)$$

where, Q is the CPE coefficient, n is the CPE exponent, ω is the angular frequency ($\omega = 2\pi f$, where f is the AC frequency) and j is the imaginary unit. CPE behaves like an ideal double layer capacitance (C_{dl}) when the value of n is 1. The correction of capacitance to its real value is calculated using eqn. 6 [15]:

$$C_{dl} = Q(\omega_{max})^{n-1} \quad (6)$$

where, ω_{max} is the frequency at which the imaginary part of impedance ($-Z_i$) has a maximum value [35].

Increase in R_{ct} values with increase in inhibitor concentration is attributed to adsorption of inhibitor molecule on the metal surface by replacing the water molecules forming a protective film on the metal surface [36,37]. Decrease in C_{dl} values in inhibited solutions compared to blank solution confirms the adsorption of inhibitor molecule on the metal surface.

Effect of temperature: From the study of temperature dependence on corrosion rate and inhibition efficiency, it is possible to calculate kinetic and thermodynamic parameters for the inhibition process which helps in interpreting the kind of adsorption behaviour followed by the inhibitor.

The energy of activation was calculated using Arrhenius equation (eqn. 7) [38]:

$$\ln(v_{corr}) = B - \frac{E_a}{RT} \quad (7)$$

where, B is a constant which depends on the metal type, R is universal gas constant and T is the absolute temperature.

Fig. 4 represents Arrhenius plots which is a plot of $\ln(v_{corr})$ vs. $(1/T)$. The slope = E_a/R was obtained from Arrhenius plots from which activation energy values were calculated. There was a decrease in energy of activation E_a with increase in concentration of the inhibitor which suggests the gradual adsorption of the inhibitor molecule on the metal surface. It is reported that lower values for E_a in inhibited solutions compared to blank is indicative of chemisorption mechanism [39].

Transition state equation was used to calculate enthalpy (ΔH^\ddagger) and entropy (ΔS^\ddagger) of activation for metal dissolution process [40].

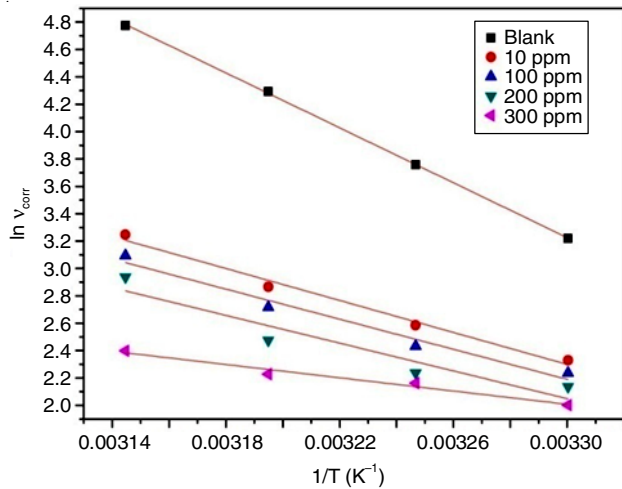


Fig. 4. Arrhenius plots for corrosion of maraging steel in 1 M HCl containing different concentrations of inhibitor

$$v_{\text{corr}} = \frac{RT}{Nh} \exp\left(\frac{\Delta S^\ddagger}{R}\right) \exp\left(\frac{-\Delta H^\ddagger}{RT}\right) \quad (8)$$

where, h is Plank's constant and N is Avagadro's number. A plot of $\ln(v_{\text{corr}}/T)$ vs. $1/T$ gives a straight line with slope = $-\Delta H/R$ and intercept = $\ln(R/Nh) + \Delta S/R$.

The positive values of enthalpy reflect endothermic nature of corrosion process. The negative values of entropy of activation indicates that the activated complex in the rate determining step represents an association rather than dissociation, resulting in decrease in randomness on going from reactant to activated complex [41]. The activation parameters are listed in Table-4.

Concentration of inhibitor (ppm)	E_a (kJ mol ⁻¹)	ΔH^\ddagger (kJ mol ⁻¹)	ΔS^\ddagger (J mol ⁻¹ K ⁻¹)
Blank	83.32	80.74	48.24
10	48.51	45.93	-74.33
100	45.64	43.06	-84.72
200	42.12	39.54	-97.50
300	20.12	17.54	-170.46

Adsorption isotherm: The value of surface coverage (θ) at different concentrations of the inhibitor was obtained from Tafel polarization studies in order to investigate the adsorption behaviour of the inhibitor on the metal surface. Surface coverage (θ) was calculated using eqn. 9 [42]:

$$\theta = \frac{\eta (\%)}{100} \quad (9)$$

where, $\eta (\%)$ is the percentage inhibition efficiency. The values obtained were tested for their fit to the experimental data using different adsorption isotherms. Langmuir Adsorption Isotherm gave the best fit which is given by the equation:

$$\frac{C_{\text{inh}}}{\theta} = C_{\text{inh}} + \frac{1}{K} \quad (10)$$

Fig. 5 shows the plot of C_{inh}/θ versus C_{inh} which gave a straight line with an intercept $1/K$.

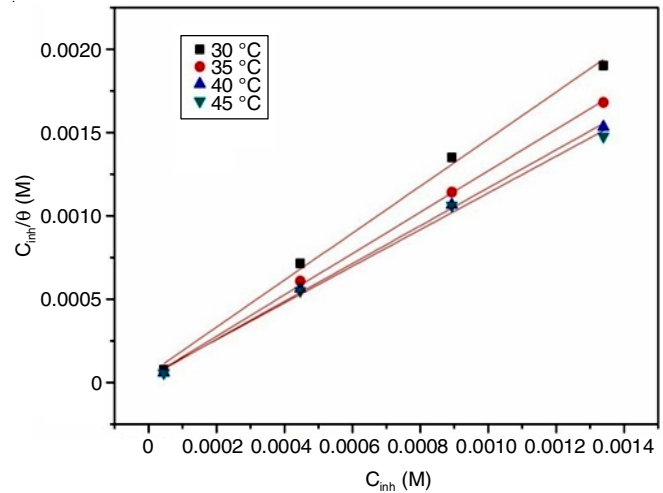


Fig. 5. Langmuir adsorption isotherms for adsorption of MTATT on maraging steel in 1 M HCl solution at different temperatures

The standard free energy of adsorption ($\Delta G^\circ_{\text{ads}}$) was calculated using eqn. 11 [31]:

$$K = \frac{1}{55.5} \exp\left(\frac{-\Delta G^\circ_{\text{ads}}}{RT}\right) \quad (11)$$

where, value 55.5 is the concentration of water in solution in mol/dm³, R is the universal gas constant and T is the absolute temperature. From the plot of ($\Delta G^\circ_{\text{ads}}$) vs. T , standard enthalpy of adsorption ($\Delta H^\circ_{\text{ads}}$) and standard entropy of adsorption ($\Delta S^\circ_{\text{ads}}$) were obtained according to thermodynamic equation (eqn. 12). The thermodynamic parameters are recorded in Table-5.

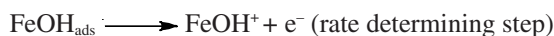
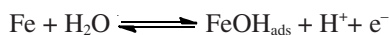
Temperature (°C)	$\Delta G^\circ_{\text{ads}}$ (kJ mol ⁻¹)	$\Delta H^\circ_{\text{ads}}$ (kJ mol ⁻¹)	$\Delta S^\circ_{\text{ads}}$ (J mol ⁻¹ K ⁻¹)
30	-36.45		
35	-38.51	13.03	165.14
40	-38.89		
45	-39.08		

$$\Delta G^\circ_{\text{ads}} = \Delta H^\circ_{\text{ads}} - T\Delta S^\circ_{\text{ads}} \quad (12)$$

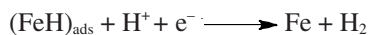
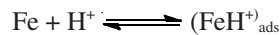
The adsorption of the inhibitor is a spontaneous process indicated by the negative value of $\Delta G^\circ_{\text{ads}}$. Studies report the value of $\Delta G^\circ_{\text{ads}}$ less than -20 kJ/mol are indicative of physisorption while those greater than -40 kJ/mol are related to chemisorption [43,44]. The present study shows both physical and chemical mode of inhibitor adsorption on metal surface indicated by values of $\Delta G^\circ_{\text{ads}}$ in the range -36.45 to -39.04 kJ/mol. Positive sign of $\Delta H^\circ_{\text{ads}}$ reveals endothermic nature of adsorption which is attributed to chemisorption. Positive value of $\Delta S^\circ_{\text{ads}}$ indicates increase in entropy during adsorption process.

Inhibition mechanism: Inhibitory effect of MTATT on the metal surface can be explained based on adsorption. Adsorption can occur due to the availability of heteroatom or π -electron cloud in the aromatic ring of the inhibitor molecule [45].

In acidic solution, the following mechanism is suggested for the corrosion of iron and steel [46].



The cathodic hydrogen evolution follows the steps:



In acidic solutions inhibitor molecule at the nitrogen atoms gets protonated and forms a positively charged inhibitor species [47]. When immersed in HCl solution containing the inhibitor the metal surface becomes negatively charged due to the adsorption of Cl^- ions and thus facilitates the electrostatic interaction with the positively charged inhibitor molecule resulting in physisorption.

Also the unprotonated inhibitor molecule may occupy vacant adsorption sites on the metal surface *via* chemisorption by sharing of electrons between heteroatom of the inhibitor and metal surface or by interaction of π -electrons of inhibitor molecule and the metal [48,49].

SEM-EDX analysis: In order to analyze the difference in surface morphology of the uninhibited and inhibited sample of maraging steel immersed in 1 M HCl, SEM-EDX investigations were carried out. Fig. 6a depicts metal surface in the absence of inhibitor and shows a rough surface with cracks and pits. Fig. 6b depicts metal surface immersed in inhibited solution and shows a smooth surface without cracks which confirms the adsorption of the inhibitor molecule on the metal surface.

Energy dispersive X-ray analyses were carried out to identify the metal composition after its immersion in 1 M HCl in the absence and presence of the inhibitor. Fig. 7a represents EDX spectrum of uninhibited sample showing absence of peak due to sulphur and atomic percentage of oxygen 54.27 % indicating formation of oxide layer. Fig. 7b represents EDX spectrum of inhibited sample showing the presence of sulphur containing peak and also atomic percentage of oxygen 47.27 % which indicates formation of sulphur containing inhibitor film on the metal surface.

Frontier molecular orbital analysis: Highest occupied molecular orbital (HOMO) energy depicts the electron donating capacity, while, energy of lowest unoccupied molecular orbital (LUMO) illustrates the electron accepting capacity, the combination of these two orbitals being called as Frontier molecular orbitals (FMOs). Therefore, higher energy value of HOMO

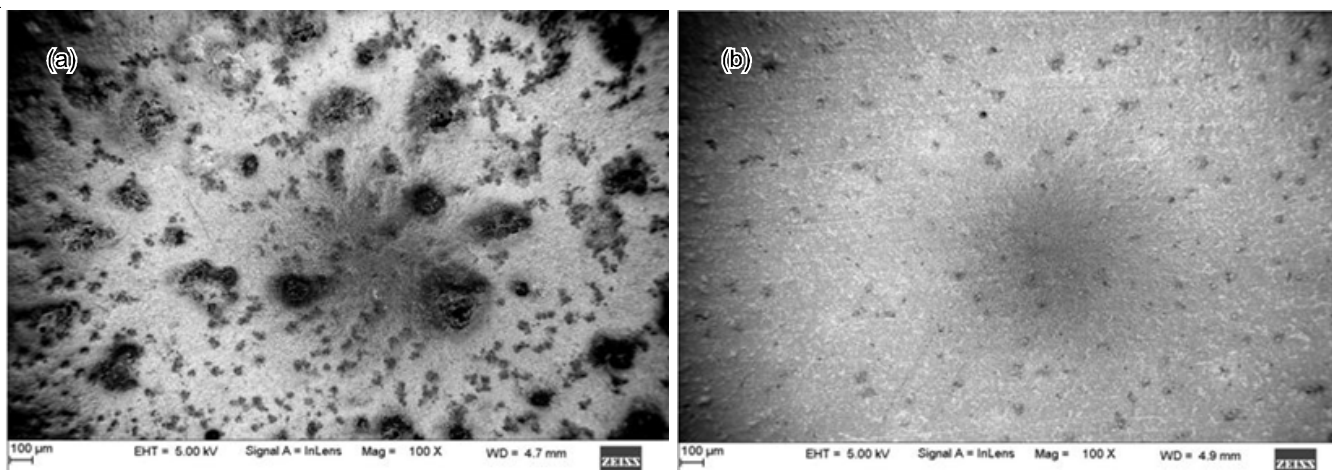


Fig. 6. SEM images of maraging steel (a) exposed to 1 M HCl solution (b) exposed to 1 M HCl solution containing 300 ppm MTATT

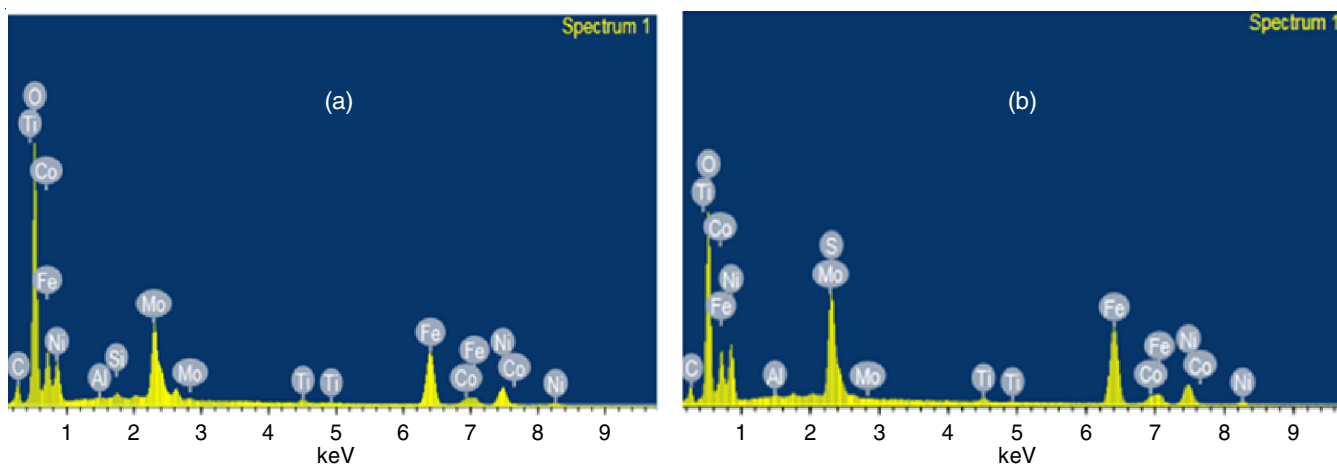


Fig. 7. EDX spectrum of maraging steel immersed in 1 M HCl (a) in absence of inhibitor and (b) in the presence of inhibitor

suggests greater ability for electron(s) donation to the acceptor molecule with lower energy and empty molecular orbital [50], while, lower energy values of LUMO describes the electron accepting tendency of the metal ions [51,52]. The chemical behaviour of a molecule is better understood in terms of $\Delta E = E_{\text{HOMO}} - E_{\text{LUMO}}$. Further, the chemical reactivity of DBTT is described in terms of various global reactivity parameters which were calculated by DFT method using B3LYP/6-311++g(d,p) basis set.

For the title compound (Fig. 8a), E_{HOMO} (MO: 58) and E_{LUMO} (MO: 59) values are -6.3960 and -2.5292 eV, respectively. The global chemical descriptors associated with present title compound are: ionization potential $I = (-E_{\text{HOMO}})$, electron affinity $A = (-E_{\text{LUMO}})$ electronegativity $\chi = (I + A)/2$, global hardness $\eta = (I - A)/2$, chemical potential $\mu = -(I + A)/2$ and electrophilicity index, $\omega = (\mu^2/2\eta)$ [53] are listed in Table-6. The HOMO-LUMO orbitals are shown in Fig. 8. From this plot it is clear that HOMO is localized over triazole ring and its methyl and thiol group, partially rest of the molecule, while the LUMO is localized over the entire molecule other than thiol and methyl groups of triazole ring.

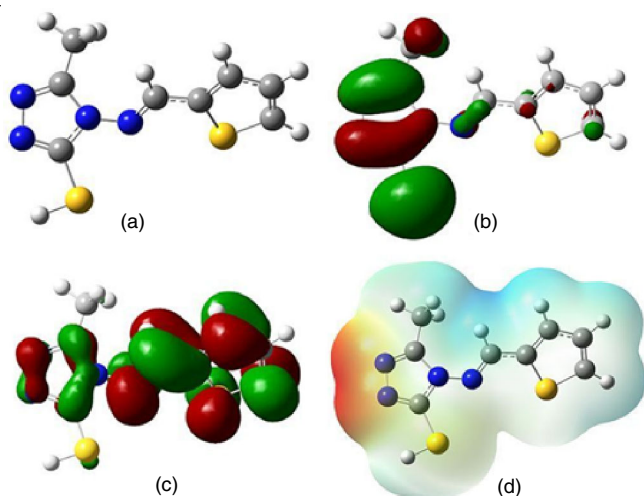


Fig. 8. (a) Optimized geometry, (b) HOMO, (c) LUMO, (d) electrostatic potential map of the title molecule

TABLE-6	
ENERGY VALUES AND OTHER PARAMETERS OF MTATT CALCULATED BY DFT/B3LYP/6-3++G(d,p) METHOD	
Parameter	Gas phase (DFT/B3LYP/6-3++G(d,p))
SCF energy (a.u)	-1325.16694730
E_{HOMO} (58) (eV)	-6.3960
E_{LUMO} (59) (eV)	-2.5292
$E_{\text{HOMO}} - E_{\text{LUMO}}$ (ΔE) (eV)	3.8668
Ionization potential ($I = -E_{\text{HOMO}}$)	6.3960
Electron affinity ($A = -E_{\text{LUMO}}$)	2.5292
Electronegativity ($\chi = (I + A)/2$)	4.4626
Global hardness ($\eta = (I - A)/2$)	1.9334
Chemical softness ($\nu = 1/\eta$)	0.5172
Chemical potential ($\mu = -(I + A)/2$)	-4.4626
Electrophilicity index ($\omega = \mu^2/2\eta$)	5.1050

From the analysis of MEP (Fig. 8d) and Mulliken atomic charges, it can be concluded that the electron rich regions have greatest ability to bind the metal surface (marked as red colour

in MEP as well as represent with more negative value in Mulliken atomic charges) while the electron poor regions have greatest ability to accept electrons (marked as blue regions in MEP as well as represent with positive value in Mulliken atomic charges). According to HSAB concept, hard acids tend to react with hard bases and soft acids actively react with soft bases. In the present case, Fe (soft acid) reacts with nitrogen atoms (C=N) of triazole ring (soft base).

Summarizing the above results, it can be concluded that the present investigated compound is able to donate electrons to unoccupied *d* orbitals of metal surface forming coordinate covalent bonds and can also accept free electrons from the metal surface by using their anti-bonding orbitals to form feedback bonds and thus, has excellent corrosion inhibition property.

Comparison: The results obtained from Tafel polarization studies and EIS studies are in good agreement as indicated by similar trend of inhibitor efficiency with increase in concentration and temperature.

Compared to the inhibitor DBAMTT studied in the previous work, the present inhibitor MTATT shows better inhibition efficiency which may be due to the presence of sulphur atom in the aldehyde moiety of the Schiff base compared to nitrogen atom in the previous inhibitor. Sulphur being less electronegative than nitrogen has a greater tendency to share its lone pair of electrons with the metal atom and thus exerts its inhibitory action.

Conclusion

Based on the results of the present study it can be summarized that synthesized Schiff base (5-methyl-4-[(*E*)-(thiophen-2-ylmethylidene)amino]-4*H*-1,2,4-triazole-3-thiol) [MTATT] acts as an efficient corrosion inhibitor on maraging steel in 1 M HCl by affecting hydrogen evolution reaction and metal dissolution thereby exerting mixed type inhibitory action. Also, efficiency of the inhibitor increases with an increase in temperature and inhibitor concentration. The mode of inhibitor adsorption follows Langmuir adsorption isotherm and results suggested that the process is chemisorption.

CONFLICT OF INTEREST

The authors declare that there is no conflict of interests regarding the publication of this article.

REFERENCES

- W. Huilong, Z. Jiashen and L. Jing, *Anti-Corros. Methods Mater.*, **49**, 127 (2002); <https://doi.org/10.1108/00035590210419371>
- S. Tamilselvi and S. Rajeswari, *Anti-Corros. Methods Mater.*, **50**, 223 (2003); <https://doi.org/10.1108/00035590310471804>
- D. Sazou, M. Pagitsas and C. Georgolios, *Electrochim. Acta*, **38**, 2321 (1993); [https://doi.org/10.1016/0013-4686\(93\)80116-H](https://doi.org/10.1016/0013-4686(93)80116-H)
- M.N. Desai and M.B. Desai, *Corros. Sci.*, **24**, 649 (1984); [https://doi.org/10.1016/0010-938X\(84\)90056-8](https://doi.org/10.1016/0010-938X(84)90056-8)
- Z.A. Iofa, V.V. Batrakov and Cho-Ngok-Ba, *Electrochim. Acta*, **9**, 1645 (1964); [https://doi.org/10.1016/0013-4686\(64\)80091-8](https://doi.org/10.1016/0013-4686(64)80091-8)
- I.B. Obot, N.O. Obi-Egbedi and S.A. Umoren, *Corros. Sci.*, **51**, 1868 (2009); <https://doi.org/10.1016/j.corsci.2009.05.017>

7. A. Quraishi, J. Rawat and M. Ajmal, *Corros. Sci.*, **54**, 996 (1998); <https://doi.org/10.5006/1.3284822>
8. M.A. Quraishi and R. Sardar, *Indian J. Chem. Technol.*, **11**, 103 (2004).
9. P. Mourya, P. Singh, A.K. Tewari, R.B. Rastogi and M.M. Singh, *Corr. Sci.*, **95**, 71 (2015); <https://doi.org/10.1016/j.corsci.2015.02.034>
10. M.A. Quraishi, R. Sardar and D. Jamal, *Mater. Chem. Phys.*, **71**, 300 (2001); [https://doi.org/10.1016/S0254-0584\(01\)00295-4](https://doi.org/10.1016/S0254-0584(01)00295-4)
11. D. Klobcar, J. Tusek, B. Taljat, L. Kosec and M. Pleterški, *Comput. Mater. Sci.*, **44**, 515 (2008); <https://doi.org/10.1016/j.commatsci.2008.04.011>
12. D.G. Lee, K.C. Jang, J.M. Kuk and I.S. Kim, *J. Mater. Process. Technol.*, **162-163**, 342 (2005); <https://doi.org/10.1016/j.jmatprotec.2005.02.102>
13. W.W. Kirk, R.A. Covert and T.P. May, *Met. Eng. Quart.*, **8**, 31 (1968).
14. G. Bellanger, *J. Nucl. Mater.*, **217**, 187 (1994); [https://doi.org/10.1016/0022-3115\(94\)90319-0](https://doi.org/10.1016/0022-3115(94)90319-0)
15. E.M. Sherif, *Appl. Surf. Sci.*, **292**, 190 (2014); <https://doi.org/10.1016/j.apsusc.2013.11.110>
16. E.M. Sherif, 15th Middle East Corrosion Conference and Exhibition, Paper No 14125m, Bahrain (2014).
17. B.S. Sanatkar, J. Nayak and A. Nityananda Shetty, *J. Coat. Technol. Res.*, **9**, 483 (2012); <https://doi.org/10.1007/s11998-011-9379-1>
18. R.N. Mary, R.A. Nazareth and P.A. Suchetan, *J. Applicable Chem.*, **7**, 171 (2018).
19. N. Shet, R.A. Nazareth and P.A. Suchetan, *Chem. Data Coll.*, **20**, 100209 (2019); <https://doi.org/10.1016/j.cdc.2019.100209>
20. L.F. Audrieth, E.S. Scott and P.S. Kippur, *J. Org. Chem.*, **19**, 733 (1954); <https://doi.org/10.1021/jo01370a006>
21. K.S. Dhaka, J. Mohan, V.K. Chadha and H.K. Pujari, *Indian J. Chem.*, **12**, 288 (1974).
22. A.D. Becke, *J. Chem. Phys.*, **98**, 5648 (1993); <https://doi.org/10.1063/1.464913>
23. C. Lee, W. Yang and R.G. Parr, *Phys. Rev. B Condens. Matter*, **37**, 785 (1988); <https://doi.org/10.1103/PhysRevB.37.785>
24. M.J. Frisch, G.W. Trucks, H.B. Schlegel, G.E. Scuseria, M.A. Robb, J.R. Cheeseman, G. Scalmani, V. Barone, B. Mennucci, G.A. Petersson, H. Nakatsuji, M. Caricato, X. Li, H.P. Hratchian, A.F. Izmaylov, J. Bloino, G. Zheng, J.L. Sonnenberg, M. Hada, M. Ehara, K. Toyota, R. Fukuda, J. Hasegawa, M. Ishida, T. Nakajima, Y. Honda, O. Kitao, H. Nakai, T. Vreven, J.A. Montgomery, Jr., J.E. Peralta, F. Ogliaro, M. Bearpark, J.J. Heyd, E. Brothers, K.N. Kudin, V.N. Staroverov, T. Keith, R. Kobayashi, J. Normand, K. Raghavachari, A. Rendell, J.C. Burant, S.S. Iyengar, J. Tomasi, M. Cossi, N. Rega, J.M. Millam, M. Klene, J.E. Knox, J.B. Cross, V. Bakken, C. Adamo, J. Jaramillo, R. Gomperts, R.E. Stratmann, O. Yazyev, A.J. Austin, R. Cammi, C. Pomelli, J.W. Ochterski, R.L. Martin, K. Morokuma, V.G. Zakrzewski, G.A. Voth, P. Salvador, J.J. Dannenberg, S. Dapprich, A.D. Daniels, O. Farkas, J.B. Foresman, J.V. Ortiz, J. Cioslowski and D.J. Fox, Gaussian, Inc., Wallingford CT, Gaussian 09, Revision B.01 (2010).
25. R. Dennington, T. Keith and J. Millam, Semichem Inc., Shawnee Mission KS, GaussView, Version 5 (2009).
26. S.K. Shetty and A.N. Shetty, *J. Mol. Liq.*, **225**, 426 (2017); <https://doi.org/10.1016/j.molliq.2016.11.037>
27. R.A. Prabhu, A.V. Shanbhag and T.V. Venkatesha, *J. Appl. Electrochem.*, **37**, 491 (2007); <https://doi.org/10.1007/s10800-006-9280-2>
28. W.H. Li, Q. He, C.L. Pei and B.R. Hou, *Electrochim. Acta*, **52**, 6386 (2007); <https://doi.org/10.1016/j.electacta.2007.04.077>
29. B.G. Ateya, B.M. Abo-Elkhair and I.A. Abdel-Hamid, *Corros. Sci.*, **16**, 163 (1976); [https://doi.org/10.1016/0010-938X\(76\)90057-3](https://doi.org/10.1016/0010-938X(76)90057-3)
30. J.M.A.E. Kader, A.A.E. Warraky and A.M.A.E. Aziz, *Br. Corros. J.*, **33**, 139 (1998); <https://doi.org/10.1179/bcj.1998.33.2.139>
31. T.S. Franklin, A. Rajesh, S. Mideen, J. Karthikeyan and S. Anitha, *Indian J. Sci. Technol.*, **5**, 2810 (2012).
32. S.K. Shukla and M.A. Quraishi, *Corros. Sci.*, **51**, 1990 (2009); <https://doi.org/10.1016/j.corsci.2009.05.020>
33. A. El-Sayed, *J. Appl. Electrochem.*, **27**, 193 (1997); <https://doi.org/10.1023/A:1018456008267>
34. X. Wang, H. Yang and F. Wang, *Corros. Sci.*, **52**, 1268 (2010); <https://doi.org/10.1016/j.corsci.2009.12.018>
35. E. Machnikova, K.H. Whitmire and N. Hackerman, *Electrochim. Acta*, **53**, 6024 (2008); <https://doi.org/10.1016/j.electacta.2008.03.021>
36. A.A. El Hosary, R.M. Saleh and M. Shams El Din, *Corros. Sci.*, **12**, 897 (1972); [https://doi.org/10.1016/S0010-938X\(72\)80098-2](https://doi.org/10.1016/S0010-938X(72)80098-2)
37. S.T. Arab, *Mater. Res. Bull.*, **43**, 510 (2008); <https://doi.org/10.1016/j.materresbull.2007.10.025>
38. T. Poornima, J. Nayak and A. Nityananda Shetty, *J. Appl. Electrochem.*, **41**, 223 (2011); <https://doi.org/10.1007/s10800-010-0227-2>
39. F. Jiajun, P. Junyi, L. Zhuo, L. Suning and Y. Wang, *Int. J. Electrochem. Sci.*, **6**, 2072 (2011).
40. S.S.A. El-Rehim, M.A.M. Ibrahim and K.F. Khaled, *J. Appl. Electrochem.*, **29**, 593 (1999); <https://doi.org/10.1023/A:1003450818083>
41. N. Soltani, M. Behpour, S.M. Ghoreishi and H. Naeimi, *Corros. Sci.*, **52**, 1351 (2010); <https://doi.org/10.1016/j.corsci.2009.11.045>
42. G.M. Pinto, J. Nayak and A.N. Shetty, *Mater. Chem. Phys.*, **125**, 628 (2011); <https://doi.org/10.1016/j.matchemphys.2010.10.006>
43. M.A. Ameer and A.M. Fekry, *Int. J. Hydrogen Energy*, **35**, 11387 (2010); <https://doi.org/10.1016/j.ijhydene.2010.07.071>
44. M.A. Ameer, A.M. Fekry, A.A. Ghoneim and F.A. Attaby, *Int. J. Electrochem. Sci.*, **5**, 1847 (2010).
45. K.F. Khaled and N. Hackerman, *Electrochim. Acta*, **48**, 2715 (2003); [https://doi.org/10.1016/S0013-4686\(03\)00318-9](https://doi.org/10.1016/S0013-4686(03)00318-9)
46. I.B. Obot, N.O. Obi-Egbedi and A.O. Eseola, *Ind. Eng. Chem. Res.*, **50**, 2098 (2011); <https://doi.org/10.1021/ie102034c>
47. G.N. Mu, X. Li and F. Li, *Mater. Chem. Phys.*, **86**, 59 (2004); <https://doi.org/10.1016/j.matchemphys.2004.01.041>
48. A.K. Satpati and P.V. Ravindran, *Mater. Chem. Phys.*, **109**, 352 (2008); <https://doi.org/10.1016/j.matchemphys.2007.12.002>
49. A. Popova, E. Sokolova, S. Raicheva and M. Christov, *Corros. Sci.*, **45**, 33 (2003); [https://doi.org/10.1016/S0010-938X\(02\)00072-0](https://doi.org/10.1016/S0010-938X(02)00072-0)
50. P. Udhayakala, T.V. Rajendiran and S. Gunasekaran, *Int. J. Adv. Sci. Res.*, **3**, 67 (2012).
51. J. Fang and J. Li, *J. Mol. Struct. (Theochem)*, **593**, 179 (2002); [https://doi.org/10.1016/S0166-1280\(02\)00316-0](https://doi.org/10.1016/S0166-1280(02)00316-0)
52. E.E. Ebenso, D.A. Isabirye and N.O. Eddy, *Int. J. Mol. Sci.*, **11**, 2473 (2010); <https://doi.org/10.3390/ijms11062473>
53. R. Parr, L. Szentpaly and S. Liu, *J. Am. Chem. Soc.*, **121**, 1922 (1999); <https://doi.org/10.1021/ja983494x>